



# Experimental proof-of-concept of the effect of inlet geometry on excavation forces and their reduction for small-scale continuous excavators

G. H. Just<sup>1,2</sup> · M. J. Roy<sup>1,3</sup> · K. H. Joy<sup>4</sup> · K. L. Smith<sup>1</sup>

Received: 12 August 2022 / Accepted: 25 March 2023 / Published online: 16 June 2023  
© The Author(s) 2023

## Abstract

Future in situ resource utilisation (ISRU) lunar mission concepts will require mechanisms that allow the available feedstock—mainly the lunar regolith—to be extracted from the lunar surface. Such extraction techniques in the reduced gravity environment of the Moon will need to minimise excavation forces, due to mass restrictions for robotic landers/vehicles and the large financial implications of placing cargo onto Earth’s satellite. An investigation of necessary excavation forces, both horizontally as well as vertically, for small-scale continuous lunar excavation systems based on their geometric inlet shapes, cutting angles, and digging depths has been undertaken. The use of vibration to disaggregate lunar soil and to reduce the necessary forces is explored as a proof-of-concept. Tests performed in a large analogue testbed have shown that the optimisation of the cutting geometry is crucial, as it inherently influences the necessary forces or even prevents deeper cuts into the soil. Our experiments indicate that shallow cuts (low digging depth) into soil at shallow angles are beneficial, and that the piling up of large surcharge masses must be avoided. Critically, applying vibration to cutting edges seems highly beneficial, as the achievable force reductions of up to 50% in the tested conditions far outweigh the additional power requirements. To make these implications immediately applicable to a wider audience, an estimation of available traction forces for certain robotic vehicles based on their mass is added for comparison.

**Keywords** Excavation · In situ resource utilisation · Lunar exploration · Rovers · Regolith · Vibration

## 1 Lunar ISRU and the need for small scale lunar excavation devices

The Moon will provide future in situ resource utilisation (ISRU) missions with a valuable feedstock in form of its powdered surface layer of soil—the lunar regolith. This material is formed from a mixture of lunar rock and minerals with an added exogenically component introduced by

various mechanisms: solar wind particles [35], asteroidal material, and cometary material [24, 27, 37]. The regolith, thus, contains a diverse range of chemical elements, which may be valuable reserves for a range of industrial and exploration applications [6, 11]. Therefore, access and extraction of the regolith are widely regarded as a key enabler of a future lunar economy and permanent human presence [11, 19, 34, 41, 42, 46], which will also enable a wide range of lunar science applications [10, 14, 16, 17, 26, 27].

At the beginning of the ISRU process chain, the geological material has to be excavated and moved to a local collection point [23, 30], and subsequently beneficiated. For early ISRU applications, that are, lunar soil particles are sorted into appropriately sized components [40]. However, the efficient and reliable excavation of regolith on the lunar surface present a significant challenge that must be overcome before lunar ISRU becomes a viable endeavour.

✉ K. L. Smith  
kate.smith@manchester.ac.uk

<sup>1</sup> School of Engineering, University of Manchester, Oxford Road, Manchester M13 9PL, UK

<sup>2</sup> ESA-European Space Research and Technology Centre, Keplerlaan, 2201 AZ Noordwijk, Netherlands

<sup>3</sup> Henry Royce Institute, University of Manchester, Oxford Road, Manchester M13 9PL, UK

<sup>4</sup> Department of Earth and Environmental Sciences, University of Manchester, Oxford Road, Manchester M13 9PL, UK

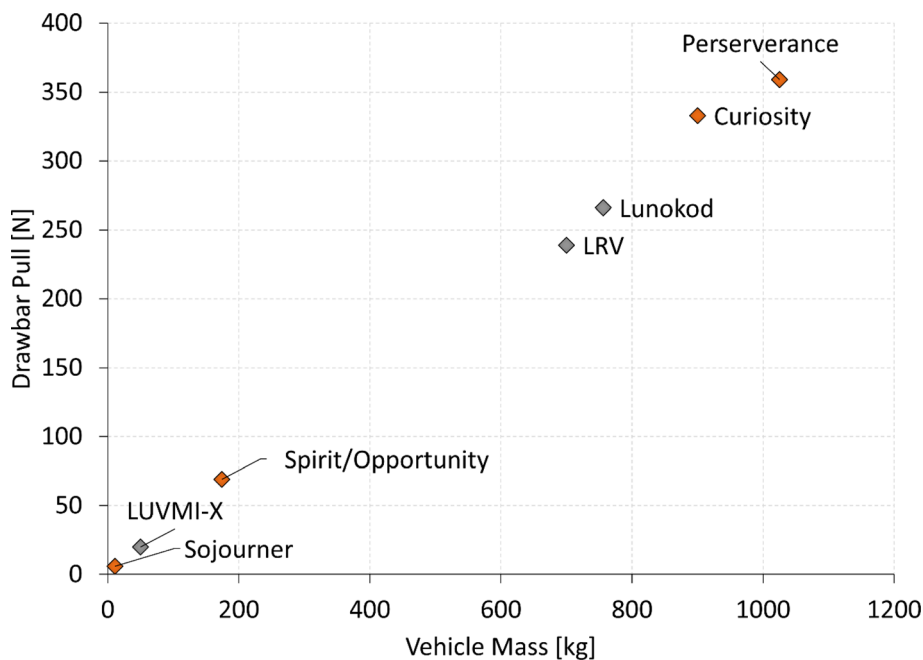


**Fig. 1** Estimation of available effective tractive force for different planetary rovers in the lunar environment. Calculations and soil data can be found in [51]. Available tractive force is based on overall system mass and ground vehicle friction parameters (such as grousers. Grousers = Devices to increase track traction, such as protrusions) are not considered. Both lunar (LRV, Lunokhod, LUVMI-X; grey markers) and martian (Sojourner, Spirit, Opportunity, Curiosity, Perseverance; orange markers) rovers are plotted for comparison

During the Apollo missions, all regolith samples were acquired by astronauts using human-operated surface sampling tools (scrapers, rakes, tongs, etc.) and sub-surface sampling tools (drills, core tubes, etc.) [4], where drilling was reported as a challenging task [50]. Working in the Moon's reduced gravity environment has a notable effect on the excavator mass required for successful extraction of the regolith [53]. On Earth, moving soil in large quantities is usually accomplished by heavy industrial machinery which utilises extensive amounts of force to achieve the given task. This mass intensity is necessary in order to counteract both lateral and vertical forces during excavation, which otherwise could lead to slipping or lifting of the excavator [53]. Given that the mass of a vehicle has a substantial effect on the available traction force and that increasing the mass of a lunar excavator would imply significant financial penalties due to increased launch costs [7], the design of lunar excavators must regard the minimisation of excavation forces as a top priority; especially for early ISRU missions involving small excavators. In a study presented by Wilkinson and DeGennaro [51], the maximum effective tractive force (defined as the difference between motion resistance and soil thrust) of the roughly 700 kg Apollo Lunar Roving Vehicle (LRV) was calculated as a mere 239 N on the Moon. Using the same soil parameters and calculations as used by Wilkinson and DeGennaro [51], Fig. 1 shows an estimation of the available effective traction force of other flown planetary rovers

on the lunar surface.<sup>1</sup> In order for a vehicle to be able to excavate material successfully, the available effective tractive force has to be multiple times larger than the necessary excavation force [18].

Thus, for excavation on planetary bodies with a reduced influence of gravity, means to reduce the necessary excavation forces must be investigated. Besides the optimisation of the cutting surface geometry, previous studies have shown that the utilisation of vibration or percussion can drastically decrease the necessary excavation forces, reaching up to a 40-times reduction in required force [9, 15, 22, 39, 44, 48, 52]. This is relevant for a lunar ISRU use-case, as a reduction in excavation forces translates directly into a possible reduction of vehicle mass or will allow the mechanism to be deployed on a smaller vehicle, which can lead to an increase in launch opportunities. Other researchers have investigated the use of vibration or electrostatics to acquire and/or convey regolith, as well as to reduce penetration forces [1, 31–33]; such techniques are not further considered in the present study as solely the decrease in excavation forces was of interest. Integrating vibrating mechanisms increases the power requirements of a given system, the potential increased rate of material fatigue must be considered, and sensitive scientific instruments must be protected accordingly. However, if significant mass savings can be achieved, the above concerns are far outweighed by the benefits.

Previous studies have investigated the effect of vibrations or more often, percussions, on discrete excavation devices (for a discussion of discrete and continuous excavators, see [30]) that push soil (i.e. bulldozing) or take one large charge at a time. To expand these approaches, this proof-of-concept study investigates four different leading-edge geometries, tests the forces necessary to excavate at different digging depths, angles, and speeds and investigates what force reductions can be achieved by utilising vibration. While a flat blade has been employed as a reference experiment (Figs. 3 and 4), the investigated leading-edge shapes are not designed to act as the actual excavation mechanism themselves (as would be the case for a discrete excavator operating in batch-mode), but rather to act as a leading-edge or an inlet interacting with the soil for use with a continuous conveying device behind them; for instance, an auger, conveyor belt, or similar technologies. The aim is to cut through the soil, lift the material of the ground with as little force as possible, and to guide it towards the back of the device where it would be transported away by a secondary conveying mechanism. For a more detailed discussion of different excavation methods and the concept of discrete and continuous excavator can be found in [30]. Such inlet shapes could be easily combined with sieves or meshes to enable the rejection of coarse particles to help beneficiation and to also mitigate the risks caused by larger rock fragments for the regolith transportation system. The decision of which leading-edge geometries to test has been based on different concepts used in terrestrial applications, such as agriculture or road clearing. It is important to highlight that the present blade shapes are not designed based on a specific set of mission requirements or for one specific excavation task, but rather aim to investigate a wide range of possible extractor designs in the present proof-of-concept study.

Small lightweight lunar robotic vehicles are currently under development, which are most likely the first candidates for carrying lunar excavation systems, for example, the LUVMI and LUVMI-X rover platforms [20, 29]. These vehicles are not designed to provide significant effective traction force, and so we have chosen to focus the test campaign towards designing a tool that can excavate the top few centimetres of soil. It is advantageous to focus on the readily powdered top centimetres of soil for ISRU applications that solely require the bulk regolith material, such as additive manufacturing [21, 55] or certain oxygen extraction methods as for instance the FFC-Metalysis process [36], unlike other processes that require specific

minerals like, for example, ilmenite for hydrogen reduction [43]. In the following, the experimental setup as well as the investigated shapes are discussed in more detail. Several studies have focussed on the mathematical modelling of necessary excavation forces [51, 53], but since most analytical models are based on specific geometric simplifications, predicting the required forces of more complex shapes is challenging. Discrete element simulation software capable of simulating solid particles, such as EDEM<sup>2</sup> or Rocky DEM,<sup>3</sup> can be applied to overcome this limitation. However, due to the small average particle size of around 72  $\mu\text{m}$  for lunar regolith [12, 49] and the wide particle size distribution from dust to cm size particles, millions of particles must be simulated, resulting in a significant demand for computing power as well as computational time. Additionally, in advance of such simulations, experimental data are necessary to calibrate the models [8]. Thus, an empirical approach is presented in this paper, serving as a proof-of-concept for the effect of leading-edge geometry on excavation forces of small-scale continuous lunar excavators and their reduction through design and application of vibration.

## 2 Experimental setup and test methods

### 2.1 Regolith analogue test bed

The test bed setup at the University of Manchester (UoM) is based on an acrylic box with inner dimensions of 100 × 60 × 30 cm. The setup is depicted in Fig. 2 and is filled with 150 kg of UoM-B lunar regolith analogue material (Fig. 2–feature a); for a full characterisation of the analogue, see [28]. The material was compacted to a filling level of 18 cm, resulting in an in situ density of roughly 1.6 g/cm<sup>3</sup>, similar to that of lunar regolith [13]. After each experiment, the soil was loosened with a rake and re-compacted to this filling level with a flat blade. Since only small excavation devices are to be tested with this arrangement, a box width of 60 cm is sufficient to avoid boundary effects, recognised as approximately three times the width of the tested implements. The same is valid for the depth of the analogue material, as cutting depths only reach up to a maximum of 5 cm [2].

A support structure (Fig. 2–feature b) for the excavation tool consists of aluminium profiles and an aluminium top shelf, connected to two housings for two linear ball bearings (Fig. 2–feature c) each, which allow the structure to slide along the rails (Fig. 2–feature d) with minimal friction while maintaining the correct orientation of the

<sup>1</sup> n.b. these estimations were performed without the effect of grousers, and several of the vehicles were deployed on Mars rather than on the Moon; however, the assessment provides a good comparison between the mass of a vehicle and its available traction force.

<sup>2</sup> <https://www.edemsimulation.com/software/>

<sup>3</sup> <https://rocky.esss.co/software/>

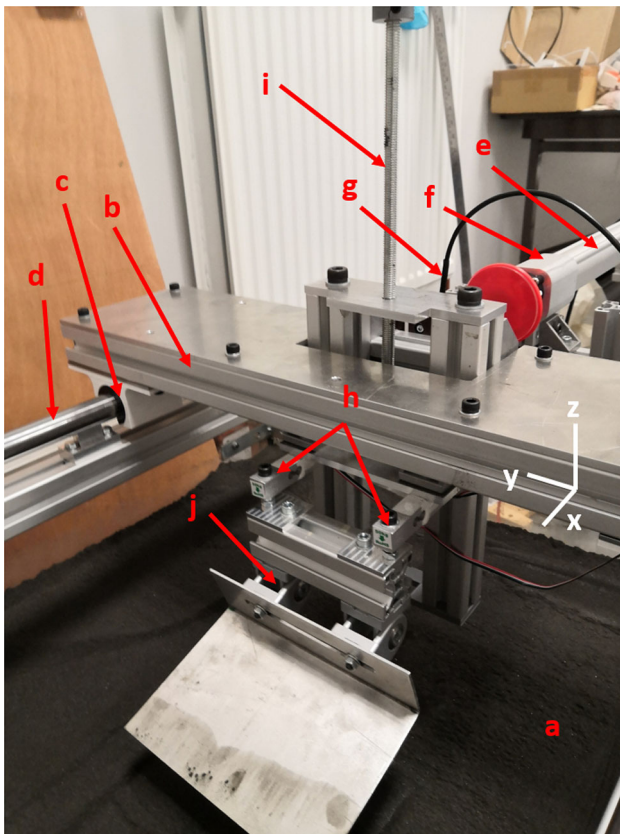


**Fig. 2** An image of the experimental setup showing the box filled with lunar analogue UoM-B (a). Features on the setup include: the support structure (b), the linear bearings and their covers (c), the guiding rails (d), the linear actuator (e) and its fixtures (f), the loadcell for horizontal excavation forces (g), the loadcells for vertical excavation forces (h), the height adjustment mechanism (i), and the lockable hinges for the cutting angle adjustment (j). Here, a flat blade is attached

experiment even during heavy loads. The support structure is pushed along the rails with the help of a 12-V DC linear actuator (Fig. 2–feature e; Gimson Robotics GLA600-S) with a maximum stroke of 700 mm and a maximum no-load speed of 21 mm/sec. The actuator is powered by an external power supply and controlled using a microcontroller and motor driver. The actuator is connected to the experiment structure with two aluminium brackets (Fig. 2–feature f; Gimson Robotics) to prevent any movement during operation. It exerts force onto a button load cell (Fig. 2–feature g; 50 kg, Phidgets) housed in a 3D-printed PLA (polylactic acid) adapter while pushing the sledge along (horizontal excavation force). The connection point for the excavation implements includes two beam load cells (Fig. 2–feature h; 50 kg, Phidgets) to be able to monitor vertical excavation forces and includes a mechanism to adjust the digging depth (i). Additionally, the digging angle can be adjusted by means of two lockable hinges (Fig. 2–feature j); digging angles were verified with

a digital inclinometer before each experiment. All three load cells are connected to HX711 signal amplifiers and the microcontroller.

An ultrasonic range finder (HC-SR04) is included in the setup, which measures the extension of the actuator, and therefore, the distance the excavation implement was pushed through the soil in each experiment. At a pre-defined distance, the experiment stopped automatically to ensure repeatable experiment runs and to prevent interference of the blade with the containment. All data were recorded at a frequency of 2 Hz, and all load cells were calibrated with precision weights prior to use. To investigate the effect of vibration, a 20-mm eccentric mass vibration motor (Precision Microdrives 320–105) was attached above the digging implement and operated at 2 V, which translates to a vibration amplitude of around 3.25 g and a frequency of 75 Hz. This setting was chosen since it is well within the envelope of the motor, allowing operation for extended periods of time, as well as due to its relative acceleration, which is calculated by

$$\Gamma = \frac{\text{applied vibrational acceleration}}{\text{ambient acceleration}}$$

and therefore results in a  $\Gamma$  of 3.25 here. The higher this value in general, the more fluidized the soil becomes. The orientation of the vibration motor can be seen, for instance, in feature E of Fig. 5. It creates mixed-mode vibrations in all directions, with the maximum amplitude being created along the x-axis (see Fig. 2 for coordinate system). It is important to note that the inclusion of vibration serves as a proof-of-concept in the present study. The specific excitation and mode imposed onto the cutting implement is domain dependent, i.e. the size, shape, mass, and material. Additionally, the imposed excitation will vary with the accumulation of soil during each experiment, as increased charges will dampen overall amplitude and eliminate higher harmonics. However, the tested shapes were not developed for one specific application and thus investigations as well as optimisations of the vibration modes, resonance frequencies, vibrational magnitudes, and frequencies of each implement lie outside the feasible scope of this initial investigation. Similar proof-of-concept studies have previously been performed by other workers, such as [9, 15], or [53], which differ to that presented here in that only one specific system or geometry was tested and that no comparisons across different geometries in the same operating conditions are drawn. Even though the presented approach does not test all possible characteristics or provide a complete vibrational analysis, it does create an initial framework from which conclusions can be drawn and design parameters for future prototypes can be derived. Therefore, the optimisation of frequency and amplitude will be the subject of future work.

**Table 1** Overview of all performed laboratory experiment runs including the maximum recorded horizontal excavation forces

Geometry	Digging angle [deg]	Digging speed [mm/sec]	Maximum horizontal excavation force [N]							
			1 cm	1 cm (vib)	2 cm	2 cm (vib)	3 cm	3 cm (vib)	4 cm	4 cm (vib)
Flat blade	15	5	8.74	6.40	22.47	18.64	42.00	38.47	72.11	73.38
		10	8.40	4.58	20.69	19.11	41.88	39.43	84.16	<b>201.22 Blade stuck</b>
	30	5	9.97	7.69	22.34	19.53	<b>44.86</b>	40.59	<b>Blade stuck</b>	<b>Blade stuck</b>
		10	10.34	8.10	29.58	26.49	<b>Blade stuck</b>	49.27	<b>Blade stuck</b>	<b>Blade stuck</b>
Bucket (0°)	15	5	4.36	3.30	12.48	9.72	22.40	18.66	N.A	N.A
		10	4.09	3.00	12.18	10.33	23.18	21.40	N.A	N.A
Bucket (15°)	15	10	5.56	4.44	15.64	14.28	32.36	28.88	N.A	N.A
Cylinder	15	10	0.89	0.44	2.71	2.15	3.95	3.45	8.06	6.54

Bold fields exceeded the safe operation limits of the setup due to the excavation implement getting stuck in the soil. The value for the flat blade at 15° and 10 mm/sec acts as an example for this. Fields labelled “N.A.” were not performed as the shapes would have likely become stuck in the soil as well as at these depths. (vib) indicates experiments that included the use of vibration

**Table 2** Overview of all performed laboratory experiment runs including the maximum recorded vertical excavation forces

Geometry	Digging angle [deg]	Digging speed [mm/sec]	Maximum vertical excavation force [N]							
			1 cm	1 cm (vib)	2 cm	2 cm (vib)	3 cm	3 cm (vib)	4 cm	4 cm (vib)
Flat blade	15	5	4.62	4.27	8.32	8.39	11.87	12.07	14.83	16.05
		10	4.35	3.73	7.75	8.51	11.49	11.83	14.90	<b>Blade stuck</b>
	30	5	2.94	2.69	4.92	5.16	6.93	7.08	<b>Blade stuck</b>	<b>Blade stuck</b>
		10	2.75	2.74	5.76	5.43	<b>Blade stuck</b>	7.30	<b>Blade stuck</b>	<b>Blade stuck</b>
Bucket (0°)	15	5	1.80	2.26	2.91	5.53	4.43	4.92	N.A	N.A
		10	1.74	1.57	2.75	3.28	4.00	4.72	N.A	N.A
Bucket (15°)	15	10	1.87	1.88	3.03	3.59	4.51	4.91	N.A	N.A
Cylinder	15	10	0.33	0.39	1.15	1.07	1.61	1.74	2.62	2.80

Bold fields exceeded the safe operation limits of the setup due to the excavation implement getting stuck in the soil. Fields labelled “N.A.” were not performed as the shapes would have likely become stuck in the soil as well as at these depths. (vib) indicates experiments that included the use of vibration

## 2.2 Investigated geometric shapes and experiment parameters

A total of 56 discrete experiments were performed, considering 4 different inlet geometries; all experiment runs are listed in Tables 1 and 2, which also report the maximum reported excavation forces per run, both horizontally as well as vertically. A flat AA 6083 aluminium alloy blade (150 mm × 80 mm × 3 mm; Figs. 2 and 3) was used to obtain reference measurements and to test the functionality of the setup. Subsequent tests used two bucket shapes with

an opening angle of 0° and 15°, respectively (100 × 80 mm for 0°; 124 × 80 mm for 15°; 3D-printed PLA; Fig. 3). As previously mentioned, the shapes are intended to act as a leading edge/inlet for a secondary conveying mechanism; therefore, the same length was chosen over the same width for the angled buckets. The final leading-edge shape tested was a cylindrical shape (50 mm inner diameter; 80 mm length; 3D-printed PLA; Fig. 3), inspired by widely used geometries for garden shovels or plow blades used in agriculture. Even though the flat blade is made from a different materials than the other

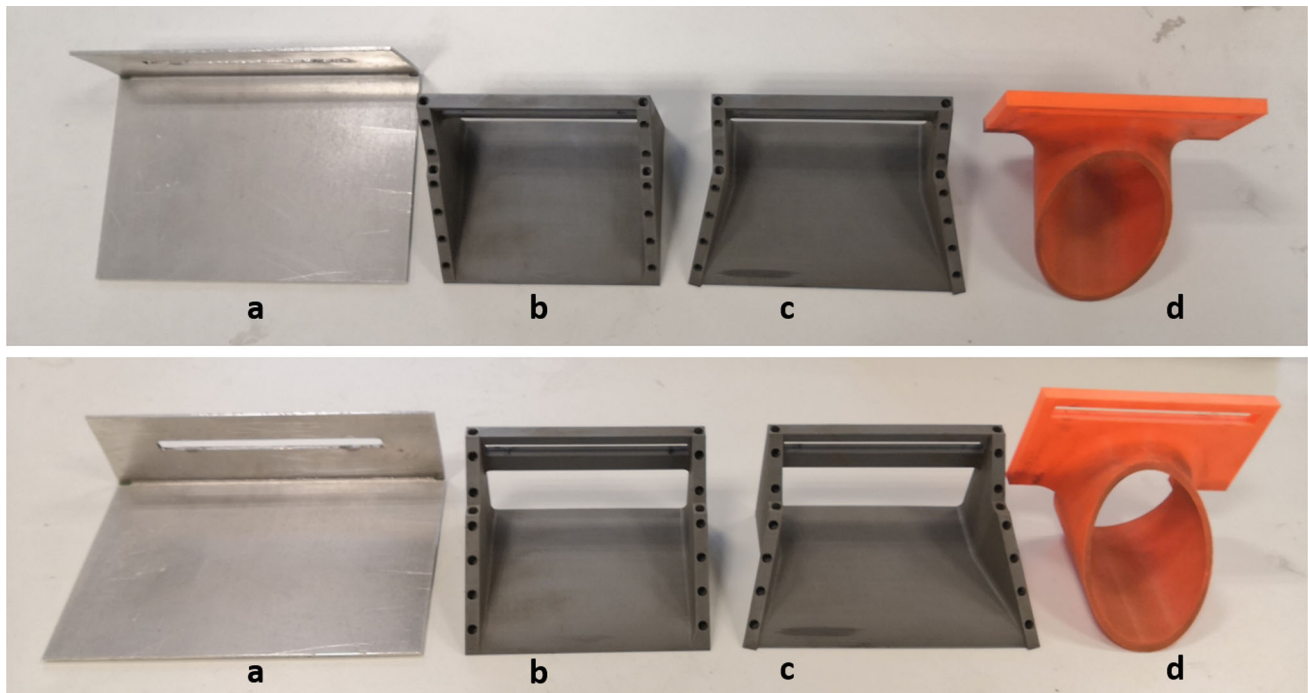


**Fig. 3** Overview of the tested geometries. **a** flat blade; aluminium; **b** straight bucket blade; PLA; **c** open bucket blade; PLA; **d** cylindrical blade; PLA. The narrow slot is used for attachment to experimental setup. The top and bottom panels in the figure show slightly different views of the blades to illustrate their back opening

geometries, due to ease of manufacture, which will of course affect the interaction between soil and material; this difference is negligible in the given circumstances. The aim is not to investigate the soil–material interaction directly at their contact point or the wear behaviour of the blades, but rather the surcharge characteristics and induced excavation forces. These are influenced more drastically by the geometry, rather than by the difference in surface roughness of two relatively smooth materials. All shapes can be seen next to each other in Fig. 3. All geometries, except the flat blade, are open at the back, as described in Sect. 2, since they are intended to be used with a secondary soil transport mechanism. The ideal outcome is reaching a force equilibrium, where the excavation forces stay relatively constant due to the material exiting the mechanism. In this case, a lunar excavator could operate continuously for extended periods of time without the need of breaking contact with the soil, and thus resulting in higher excavation rates. Terrestrially, excavator leading edges are often equipped with teeth to facilitate excavation; such features could be beneficial, as discussed in [25] but were not included in the present study due to the focus on excavation forces caused by different geometries.

The digging depth was adjusted in 1 cm steps with cuts at 3 to 4 cm already resulting in the flat blade getting stuck in the soil, leading to a sharp increase in excavation forces which could eventually damage the actuator or other

components. Some experiments exceeded horizontal excavation forces of 200 N, which given the small size of the tested geometries and the shallow digging depths, is excessive (see Table 1 for an example of this). For a lunar rover, such forces could have catastrophic consequences, as the momentum on the rover would be significant and could lead to it tipping over, resulting in mission failure. Thus, except for two experimental runs, only digging depths up to 3 cm are considered here. Two different cutting angles were investigated, namely 15° and 30°, measured against the horizontal plane of the soil surface. Lastly, runs were performed at different actuator speeds of 10 mm/sec and 5 mm/sec, as well as with and without vibration. During the experiments, the digging implements travelled approximately 41 cm through the soil.

### 3 Results

Tables 1 and 2 show an overview of all performed experiment runs, where experiments with excavation forces exceeding the safe limits due to the digging implement getting stuck in the soil are greyed out.

The initial experiments with the flat blade were performed up to 4 cm digging depth, but it became apparent that the deepest cuts already lead to immense forces acting on the excavation implement. Thus, this depth was not

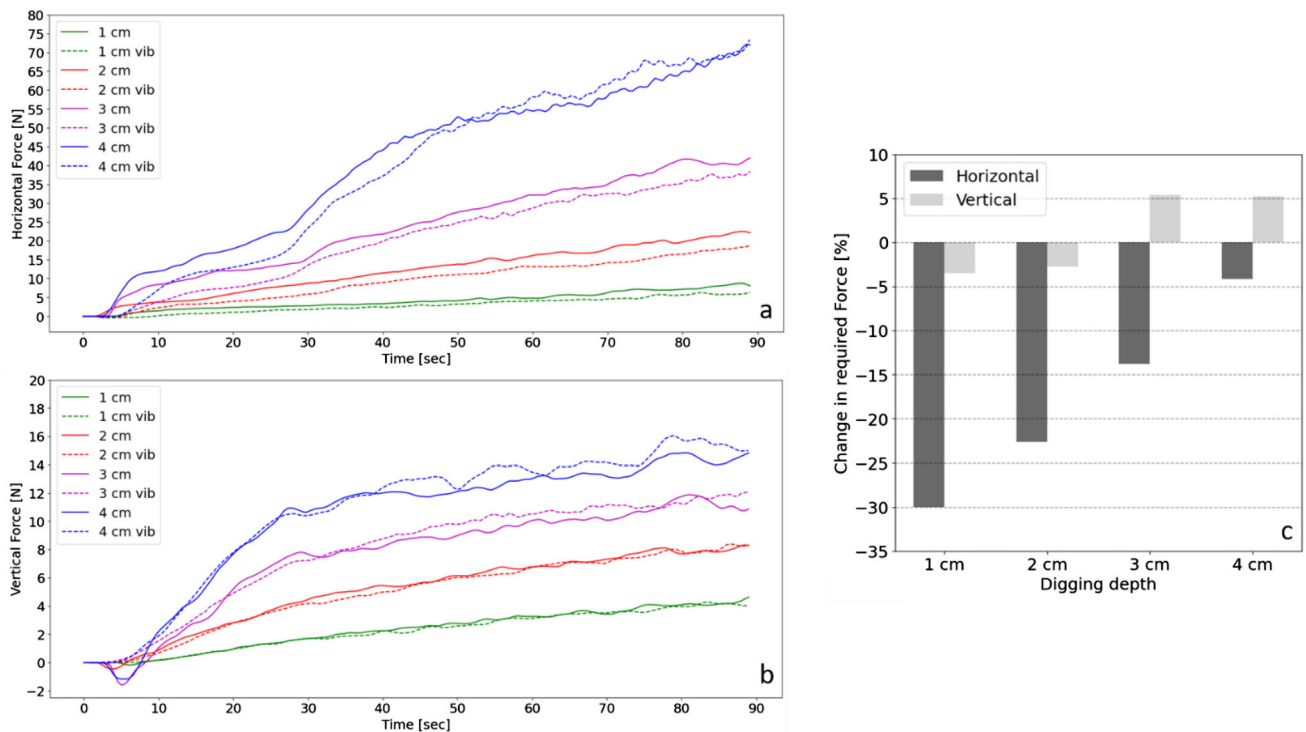


**Fig. 4** Recorded horizontal (a) and vertical (b) excavation forces for the flat blade at  $15^\circ$  cutting angle and a cutting speed of 5 mm/sec. The bar chart (c) shows the change in necessary forces when using vibration. Raw data reported in supplementary Figure S1

tested for the other bucket shapes as similar results would have been expected; therefore, these are labelled “N.A.” in Tables 1 and 2. Before each set of experiments, a reference run was performed with and without vibration (no contact to the soil, but with the same configuration in terms of angle and speed). The required forces for these runs, representing the force necessary to overcome the friction in the system, was subsequently subtracted from the force curve of runs with soil contact. Therefore, the forces evaluated below represent the actual forces induced by the excavation operation and are independent of the friction of the system.

### 3.1 Flat blade

Figures 4, 6, 7, and 8 show the recorded excavation forces for the different runs at different digging depths. Experiments without the use of vibration are shown in solid lines and dashed lines indicate the use of vibration. These figures show a 3-step moving average of the raw data, which can be found in the supplementary information to this publication. The bar charts shown indicate the change in necessary excavation forces, both horizontally as well as vertically, when utilising vibration. The percentage change was calculated by computing the area below the force-time curves, which are reported across identical time spans. Comparing these values allows for a comparison of the

overall force required for the whole run. This, combined with the reported peak forces in Tables 1 and 2, gives a valid indication of the required overall forces.

Our results (Fig. 4, Tables 1 and 2) show that the use of vibration reduces the horizontal excavation force significantly, up to around 30% for a shallow cut at 1 cm. This decrease in required force becomes less significant with increasing digging depth; however, the reduction is still noteworthy. The use of vibration delays the rise in horizontal excavation forces, as the surcharge is hindered from piling up due to material flowing more easily, which becomes more apparent at increased digging depths. Interestingly, the required horizontal excavation force at 4 cm depth with vibration surpasses the one without at a certain point, which could be caused by the increasing surcharge mass acting as a damper for the vibration or changing the vibration mode, and thus preventing any further force reduction. For detailed discussions of the soil mechanics involved in the creation of surcharges, see [3, 38, 54]. Regarding the vertical excavation forces, vibration do not significantly decrease the required forces. For deeper cuts (3 to 4 cm), the vertical excavation force even increases with the use of vibration, as the surcharge is compacted by the effects of the vibration. The cyclic behaviour visible for both excavation forces, which becomes more apparent for deeper cuts (3 to 4 cm), is caused by the surcharge piling up (increase in force) and

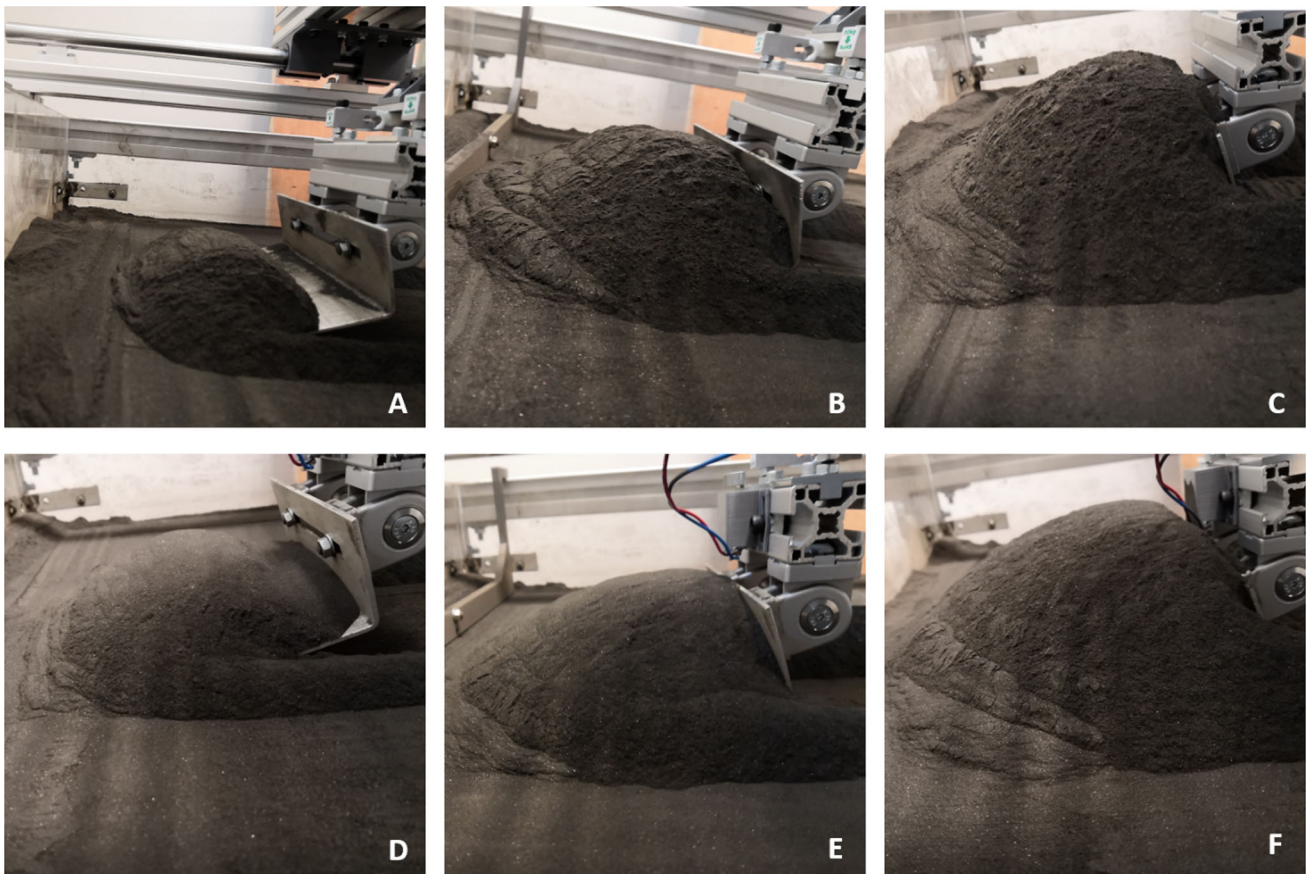


**Fig. 5** Images of the surcharge after experiments with a flat blade at  $15^\circ$  cutting angle and at 5 mm/sec. **A** 1 cm, no vibration; **B** 2 cm, no vibration; **C** 3 cm, no vibration; **D** 1 cm, vibration; **E** 2 cm, vibration; **F** 3 cm, vibration

then suddenly breaking loose and moving forwards (decrease in force). A similar behaviour can be observed in most of the data in the following. Some of these described phenomena can be seen in Fig. 5, showing images of the surcharge after the described test at digging depths of 1 to 3 cm, with (A–C) and without (D–F) vibration.

As the excavation speed was increased (Fig. 6), a primary observation is that a cut at 4 cm depth with the use of vibration resulted in the blade getting stuck (see Tables 1 and 2). This is a result of the already high horizontal excavation force of around 85 N and the increase in vertical excavation force with vibration, as shown above. This combination leads to the blade changing its cutting angle due to the significant momentum acting on it, which in turn makes the problem even more severe as the cutting angle increases. Overall, the maximum required forces for cuts up to 2 cm are lower compared to a slower cut at the same angle and almost similar at deeper cuts. The use of vibration again reduces the horizontal excavation force but increases the vertical excavation forces at deeper cuts. The decrease in the horizontal excavation force for a shallow 1 cm cut is significant, as it almost halves the required overall force.

Figure 7 shows the results for an increased cutting angle of  $30^\circ$ . Overall, the required horizontal excavation force increases compared to the same speed at a lower cutting angle and cuts at 4 cm are not possible at all anymore. Since the blade angle is now steeper, the blade cuts less well through the soil but rather displays a pushing or plowing motion, leading to a steep increase in the required force and would therefore exert a significant momentum on any vehicle. Vibration reduces the required horizontal excavation force significantly, even more than at a slower speed (Tables 1 and 2). Overall, a decrease in required vertical excavation force can be observed compared to the same speed at  $15^\circ$ , as less soil accumulates on top of the blade. This is caused both by the steeper blade angle as well as the pushing motion that lofts less material off the ground.

Similar observations can be made for a cut at a high angle and with a higher speed (Fig. 8). Here, already a 3 cm cut without the use of vibration is not possible anymore and the forces are significantly higher than for both the same digging angle at slower speeds, as well as the same speed at a lower cutting angle. Nevertheless, the use of vibration decreases the necessary horizontal excavation



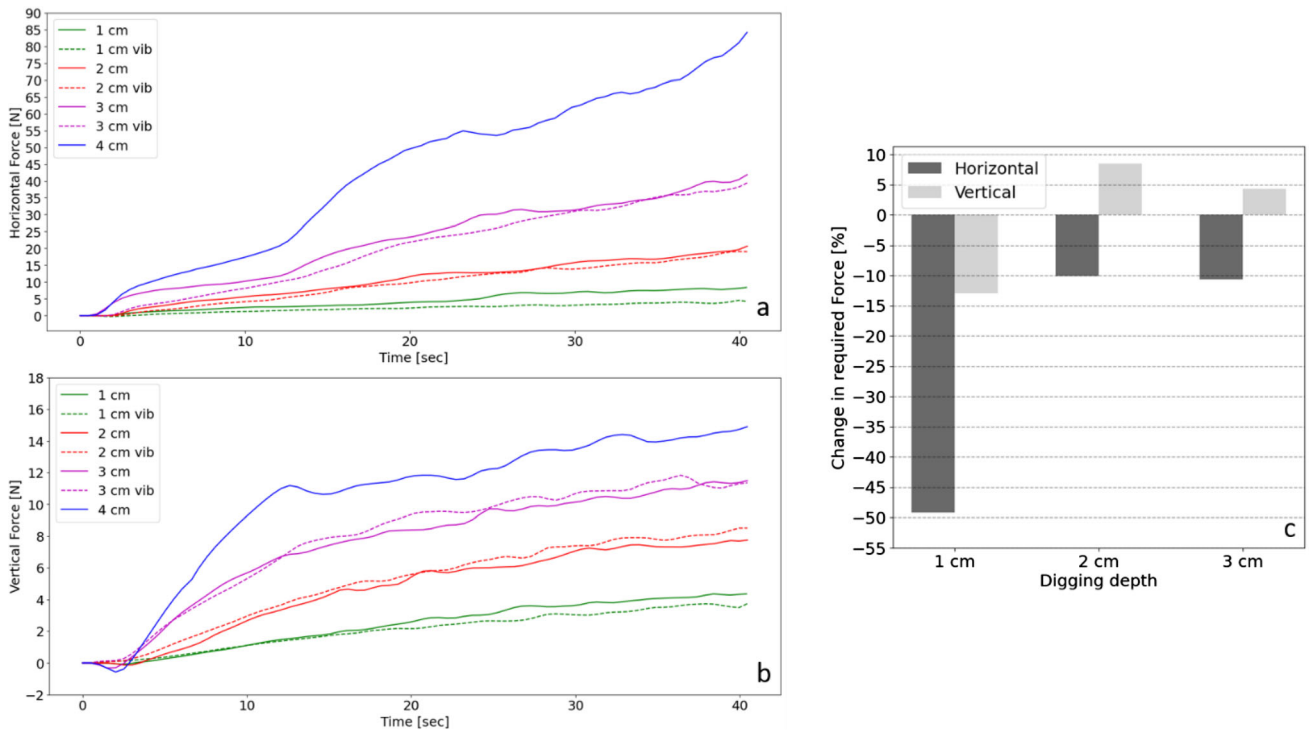


**Fig. 6** Recorded horizontal (a) and vertical (b) excavation forces for the flat blade at 15° cutting angle and a cutting speed of 10 mm/sec. The bar chart (c) shows the change in necessary forces when using vibration. Raw data reported in supplementary Figure S2

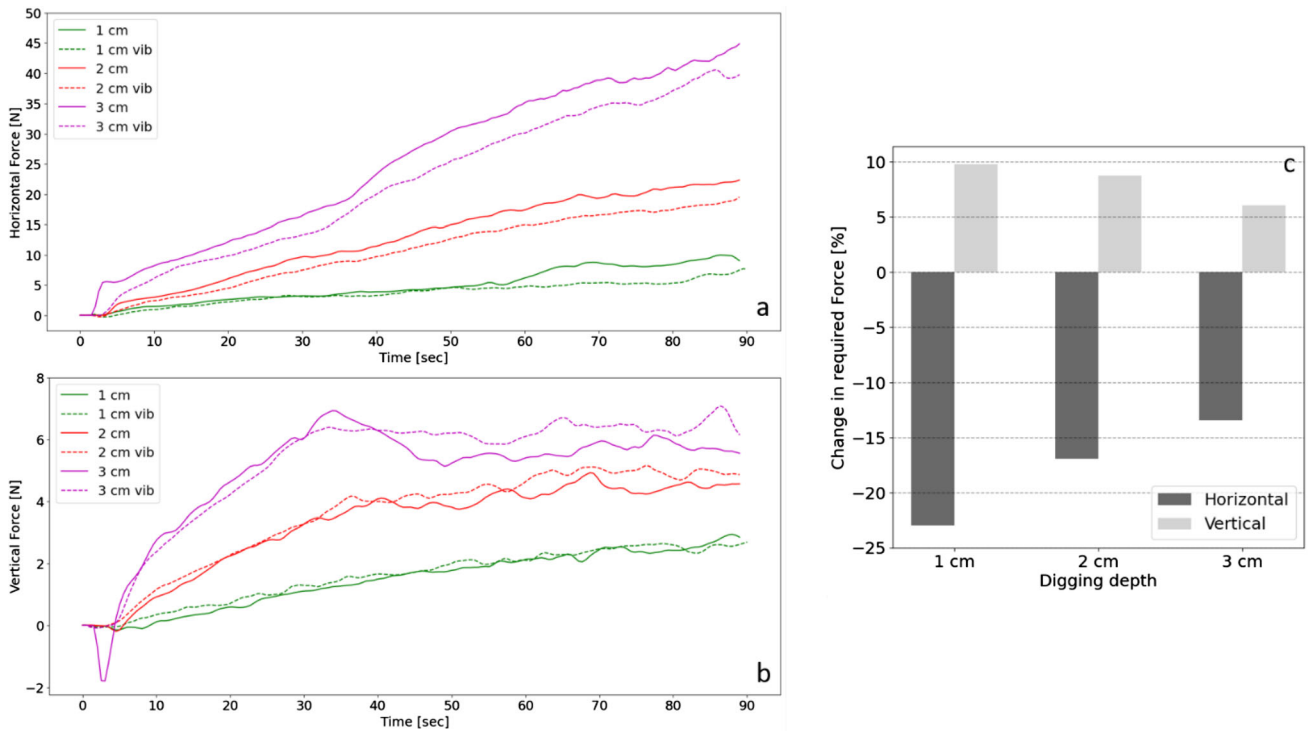


**Fig. 7** Recorded horizontal (a) and vertical (b) excavation forces for the flat blade at 30° cutting angle and a cutting speed of 5 mm/sec. The bar chart (c) shows the change in necessary forces when using vibration. Raw data reported in supplementary Figure S3

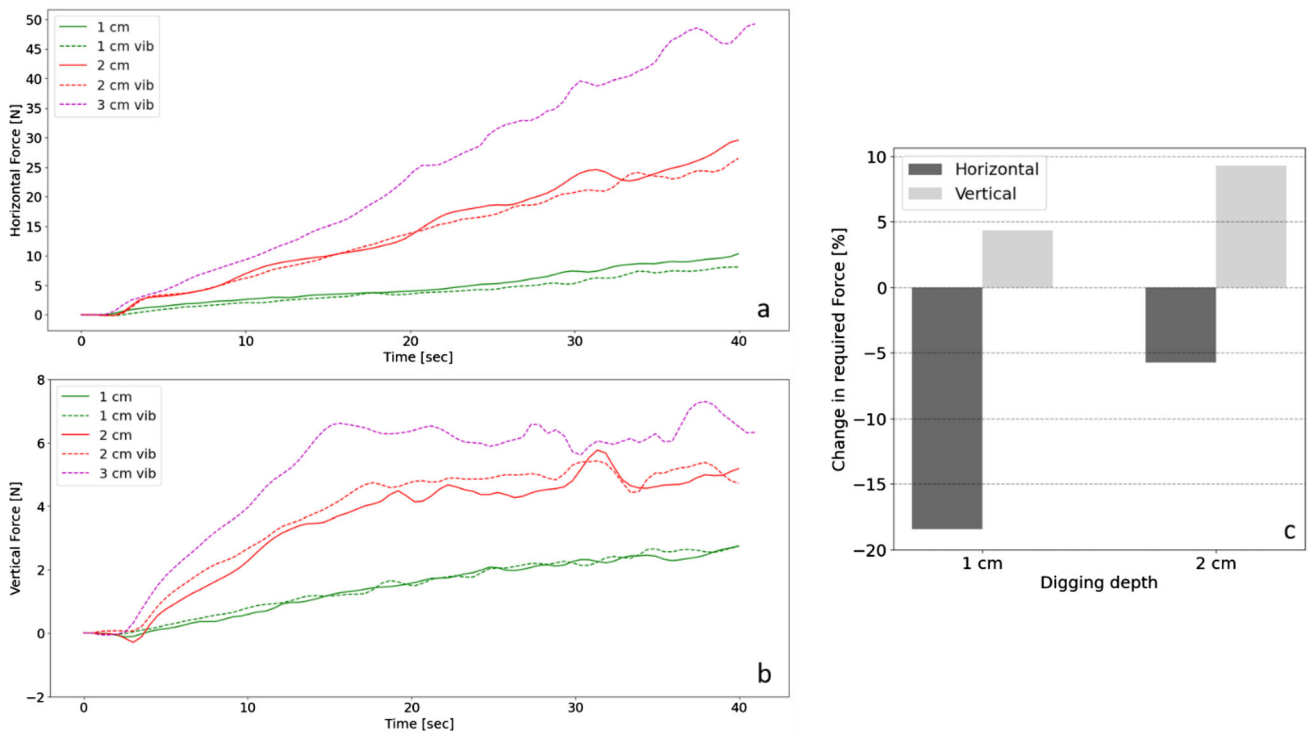


**Fig. 8** Recorded horizontal (a) and vertical (b) excavation forces for the flat blade at 30° cutting angle and a cutting speed of 10 mm/sec. The bar chart (c) shows the change in necessary forces when using vibration. Raw data reported in supplementary Figure S4

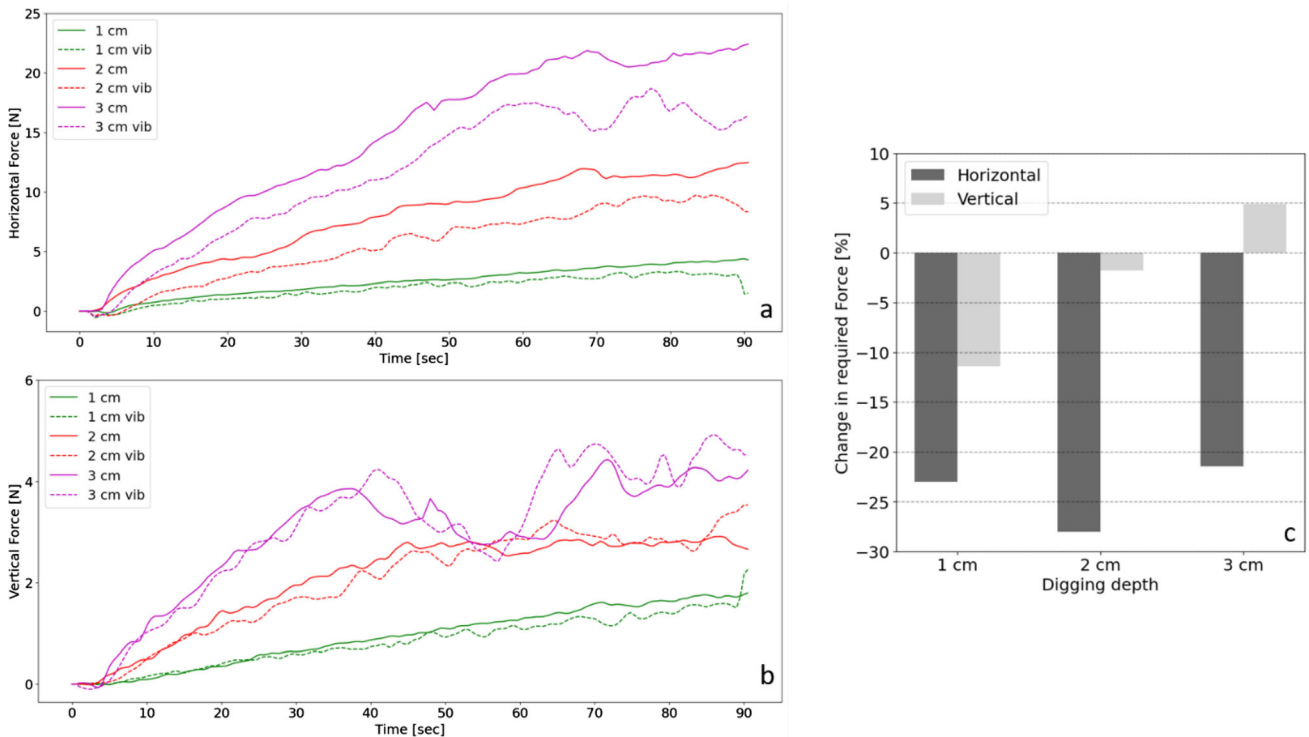


**Fig. 9** Recorded horizontal (a) and vertical (b) excavation forces for the straight bucket at 15° cutting angle and a cutting speed of 5 mm/sec. The bar chart (c) shows the change in necessary forces when using vibration. Raw data reported in supplementary Figure S5

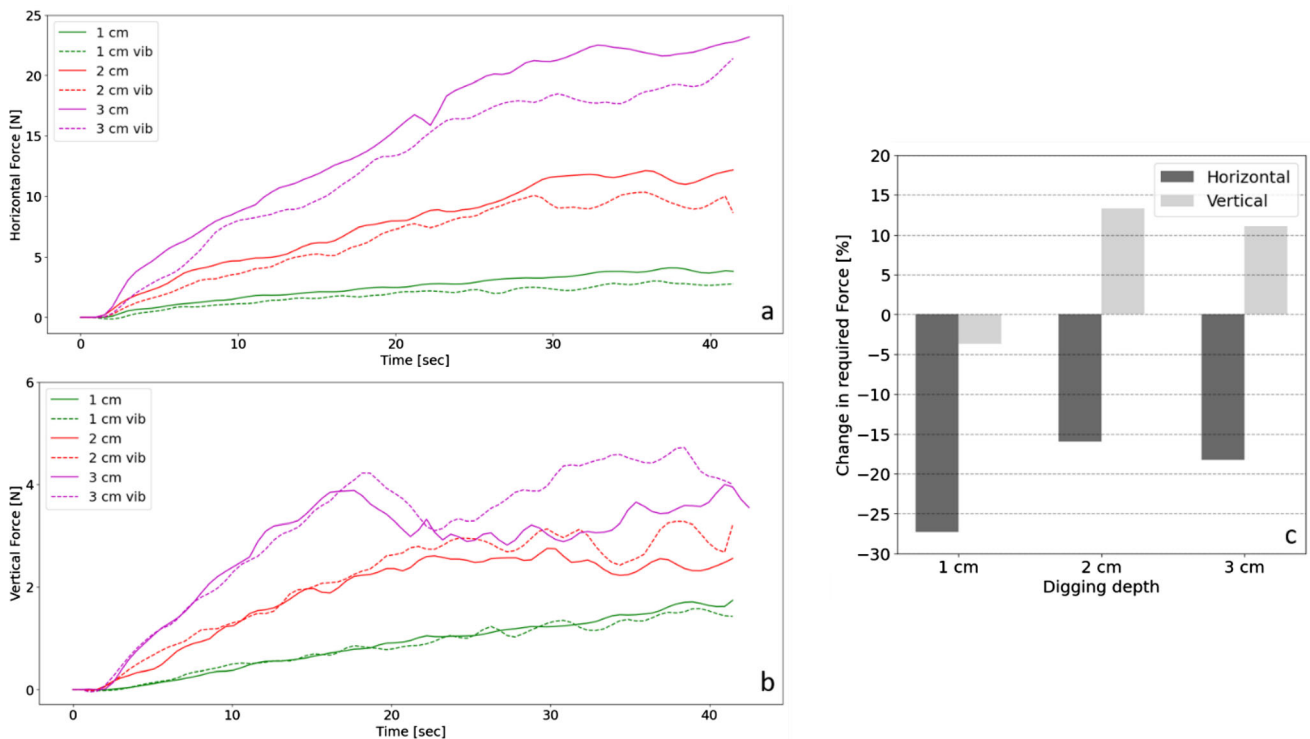
forces but increases the vertical excavation forces; this is consistent with the observations from the runs described above.

In summary, our findings suggest that shallow cuts (1 to 2 cm) at a low cutting angle ( $15^\circ$ ) with a slightly increased excavation speed (10 mm/sec) result in the lowest overall excavation forces. The effects of using vibration to reduce excavation forces are significant (up to 50% force reduction), and therefore, are worth the increased demand in power. It is apparent that steep cutting angles ( $30^\circ$ ), even with the use of vibration, are detrimental for the given use case as they increase the necessary forces and additionally increase the risk of the digging implement getting stuck in the soil. Taking these findings into consideration, all of our remaining experiments were performed at a cutting angle of  $15^\circ$ . The high overall excavation forces for even a very small digging implement and relatively shallow cuts, which increase linearly with the digging depth, show that discrete excavation with a flat blade or bulldozing does not seem applicable for a lunar use case where low excavation forces are critical.

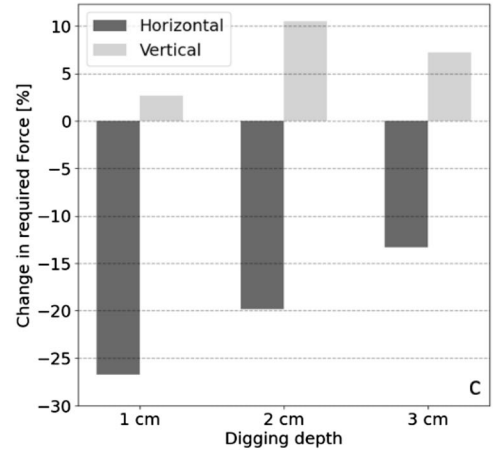
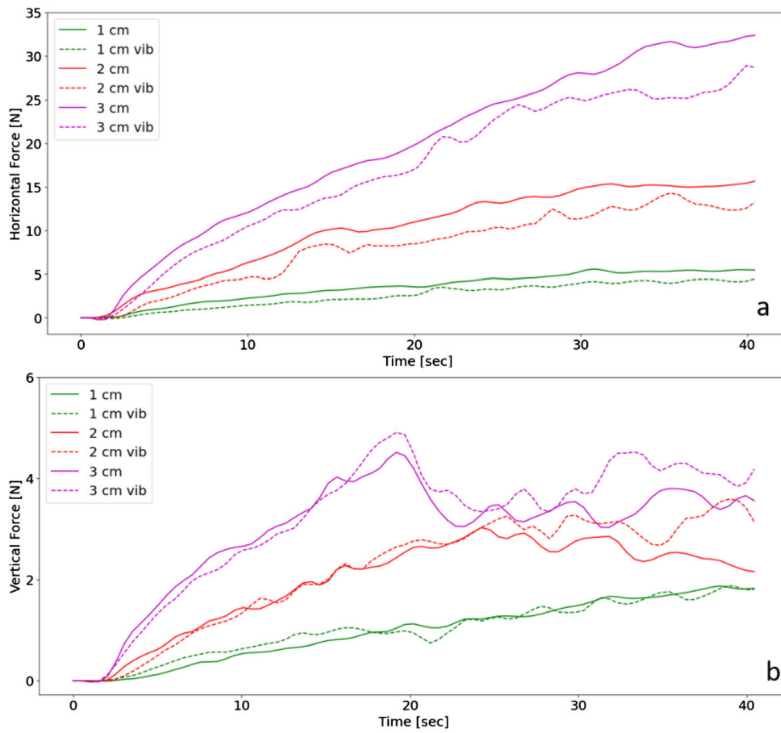
### 3.2 Straight bucket blade ( $0^\circ$ opening)

Figure 9 shows the results for the straight bucket (as depicted in Fig. 3b) at a  $15^\circ$  cutting angle and for a speed of 5 mm/sec, and Fig. 10 shows the same shape at a speed

of 10 mm/sec (data are reported in Tables 1 & 2). Overall, the peak forces for this shape are significantly lower than for a flat blade. We attribute this to the shape cutting through the soil more easily, thus reducing the surcharge mass, reduced width, as well as a reduced surcharge mass as the material is allowed to leave the excavation implement easily (Fig. 3b). The latter starts to take an effect from 2 cm digging depth, as there is not enough material excavated at 1 cm to reach the end of the geometry. Vibration increases the amount of material exiting the geometry as it increases the flowability of the soil. As previously mentioned, ideally the force curve would level off and stay relatively constant. Even though this equilibrium of forces is not reached here yet, it is visible in Fig. 10 that the required force is starting to level out once enough material exits the mechanism. This is especially apparent in the recorded values for the vertical excavation forces. While vibration again helps to reduce the horizontal excavation forces significantly, it can be seen that shallow and slightly faster cuts are beneficial, unless deeper cuts are targeted. Deeper cuts, however, seem disadvantageous since it increases the required forces significantly. In general, enough material must be excavated to reach the end of the geometry in order to develop the full force reducing potential of the geometry and to feed the material to the secondary mechanism. This makes a trade-off between the amount of excavated material and force required necessary.



**Fig. 10** Recorded horizontal (a) and vertical (b) excavation forces for the straight bucket at  $15^\circ$  cutting angle and a cutting speed of 10 mm/sec. The bar chart (c) shows the change in necessary forces when using vibration. Raw data reported in supplementary Figure S6



**Fig. 11** Recorded horizontal (a) and vertical (b) excavation forces for a bucket with 15° opening at 15° cutting angle and a cutting speed of 10 mm/sec. The bar chart (c) shows the change in necessary forces when using vibration. Raw data reported in supplementary Figure S7

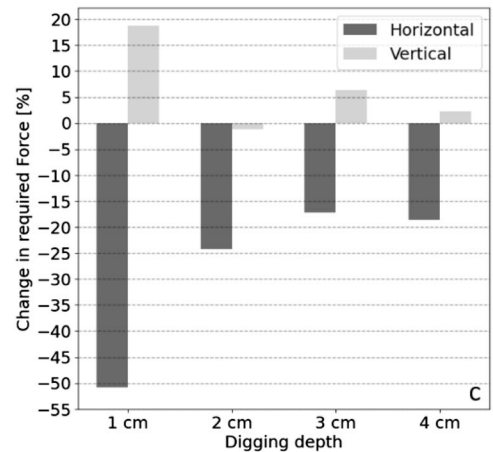
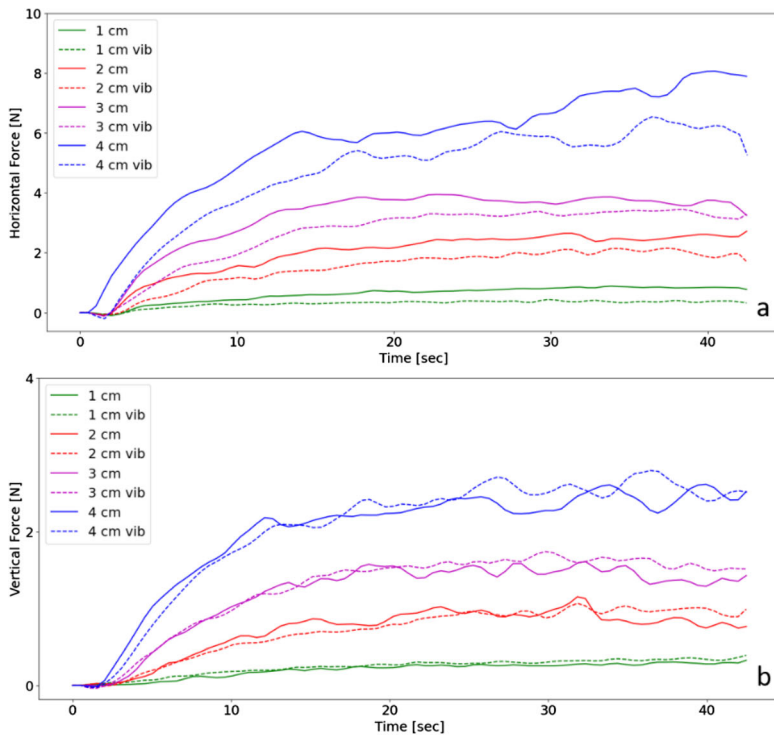


**Fig. 12** Recorded horizontal (a) and vertical (b) excavation forces for a cylindrical shaped blade at 15° cutting angle and a cutting speed of 10 mm/sec. The bar chart (c) shows the change in necessary forces when using vibration. Raw data reported in supplementary Figure S8

Two additional verification runs were performed at a 5° cutting angle and one at 15 mm/sec, which both resulted in additional force reductions. Because of this clear relationship between angle, speed, and required force, subsequent experiments were performed at a 15° cutting angle and a speed of 10 mm/sec to allow for a good comparison to prior results utilising the flat blade.

### 3.3 Open bucket blade (15° opening)

Figure 11 shows the result for the bucket geometry with an opening angle of 15° (as depicted in Fig. 3c). Generally, the results show a very similar behaviour compared to the bucket with straight walls (Fig. 10). However, more material is piled up in front of the geometry due to the increased projected area of the side walls and thus the required forces are higher overall by 20–30% for the horizontal forces (Table 1) and 10–20% for the vertical forces (Table 2). This emphasises once more that shapes that increase the amount of surcharge produced while excavating must be avoided, even though they would allow for more material being gathered in one cut.

### 3.4 Cylindrical blade

Lastly, a cylindrical blade shape (as depicted in Fig. 3d) was tested and the results can be seen in Fig. 12. It is apparent that the peak forces required are significantly lower (up to  $\times 10$  compared to the bucket shapes; up to  $\times 11$  compared to the flat blade; see Tables 1 and 2) than for any other experimental run, even at an increased cutting depth of 4 cm and that vibration reduce the necessary horizontal excavation force drastically, especially at low digging depths. From a depth of cut of 2 cm onwards, the material begins to reach the end of the geometry and the forces required reach the abovementioned force equilibrium relatively quickly. At 3 cm, the cylinder is almost fully submerged in the soil and would therefore excavate the maximum possible mass. The increase in horizontal excavation force at 4 cm is caused by the geometry being overfilled, thus creating additional contact surfaces between the top of the inlet and the soil.

In general, the rounded and narrow shape with a tipped leading edge (Fig. 3d) is by far advantageous compared to more rectangular shapes as it produces almost no surcharge and transports the material off the ground with ease. Even though this is not overly surprising, many proposed lunar excavator designs today utilise buckets or similar rectangular shapes [30]. The digging depth here should be adjusted in a way that the geometry is almost fully submerged in the material to maximise the throughput.

## 4 Conclusion

In this proof-of-concept study, four different geometric shapes (Fig. 3), representative of possible leading-edge options for lunar excavators with a secondary transport mechanism, have been investigated in a planetary analogue testbed at the University of Manchester. Tests were performed at two different cutting angles, two excavation speeds, and with and without the use of vibration. The presented research shows clearly that shape optimisation of digging implements or excavator inlet geometries for lunar excavation devices must be considered from the beginning of the conceptual design phase. During the performed experiments, horizontal excavation forces varied by more than an order of magnitude between a flat blade and a cylindrical inlet design.

It has been found that bulldozing with a flat blade or a closed bucket is not sensible for lunar applications, where excavation forces must be held to a minimum due to the reduced gravity environment and significant launch costs. The created surcharge causes sharp increases in the necessary forces and even cuts at only a couple of centimetres could not be performed by the robotic vehicles we are utilising today (see Fig. 1); thus, surcharge mass must be kept to a minimum.

Instead of closed blade geometries, the present study shows that lunar excavator designs shall be optimised for the secondary regolith transportation mechanism they are utilising. This can either be achieved with multiple small cutting surfaces that scoop up the soil and store it inside the vehicle, like for instance a bucket wheel excavator as described in [45] or by designing them in a way that excavated material can be transported away from the inlet by an auger, mechanical, or pneumatic conveyer system continuously. This will enable also small robotic vehicles to contribute to the development of future lunar ISRU capabilities. Additionally, multiple shallow cuts at shallow angles should be targeted wherever possible as the necessary forces increase substantially with increasing digging depth and steeper angles. On the lunar surface, this effect will be even more drastic due to the compaction and quickly increasing relative density of the regolith layer [24]. Different inlet geometries will, of course, lead to different excavation mass rates, different surcharge masses, and will affect the required forces differently, which must be considered and optimised for future lunar applications; such investigations are subject of future work as measuring the excavated mass accurately, in situ, and without affecting the excavation forces in a large-scale experiment that focuses on the top few centimetres of the soil is extremely challenging. Therefore, the aim is not to recommend one specific geometry, but rather create a

reference framework on which new designs can be based. Thus, the present results demonstrate clear trends across a wide range of possible shapes that should be considered in the design of any excavation implement.

The presented tests were performed under Earth's gravity and environmental conditions (i.e., pressure) and thus the excavation forces on other celestial bodies or planets will be different, as research indicates that the mechanical behaviour of soils changes in altered gravity conditions [5, 47, 56]. Thus, developments of excavation devices for certain gravitational environments should be complemented with simulations, which allow to change the gravitational acceleration easily, as well as, for instance, parabolic flights for experimental verification.

Critically, applying vibration to cutting edges seems highly beneficial, as the achievable force reduction of up to 50% in the arrangements considered, far outweigh the additional power requirements for excitation. Here, the use of vibration was used as a proof-of-concept, which resulted in significant reductions of necessary forces. However, with optimised vibrational profiles, which are specifically tailored to a specific geometry, implement size, and mass, it is tenable that the required forces could be reduced even further. Such optimisation efforts are only reasonable, however, after a final geometry is chosen for a specific application as slight geometry changes would lead to the need of a full re-characterisation of the vibrational characteristics. In addition, vibration facilitates the clearing of residue material off the cutting surfaces; this is in good accordance with the results reported by, for example, [53].

In the presented experimental study, the omni-directional vibration motor was attached above the cutting implement (as seen in Fig. 5), since different geometries had to be attachable readily, and their cutting angle had to be changed freely. Although the vibration used here acted as a proof-of-concept, for future vibrational actuation of leading edges, we propose the use of linear resonant actuators (LRA), as these allow the direction of vibration in a single axis and thus enable investigations into the optimum vibration direction (horizontal only vs. vertical only vs. combination of both). Additionally, attaching the actuator directly to, or incorporating it into, the chosen leading-edge geometry seems beneficial and simplifies a detailed examination of the vibration mode of the geometry.

In summary, it is found that small robotic soil excavation devices should be equipped with inlets or leading edges that are optimised for the present use-case and environment, and simply miniaturising terrestrial concepts will not be beneficial or not even feasible for many applications. The comparison of the reported forces to the available traction of several robotic vehicles also shows,

that we are currently still far away from large-scale excavation endeavours on the lunar surface.

**Supplementary Information** The online version contains supplementary material available at <https://doi.org/10.1007/s11440-023-01914-4>.

**Acknowledgements** Gunter H. Just acknowledges the support of the University of Manchester's EPSRC Doctoral Training Partnership, ESA's Network & Partnership Initiative (4000130229/20/NL/MH/hm), and by the FAIR-SPACE Hub (RN0344). Katherine H. Joy is supported by the Science and Technology Facilities Council (ST/R000751/1), the Royal Society (URFR\201009), and the Leverhulme Trust (RPG-2019-222). M. J. Roy acknowledges support from the EPSRC (EP/L01680X/1) through the Materials for Demanding Environments Centre for Doctoral Training, as well as the FAIR-SPACE Hub (RN0344). K. L. Smith acknowledges support from the FAIR-SPACE Hub (RN0344). We would like to thank the three reviewers for their constructive comments that we believe helped to improve the quality of this manuscript substantially, as well as the associate editor for their guidance.

**Data availability** Some or all data, models, or code that support the findings of this study are available from the corresponding author upon reasonable request.

## Declarations

**Conflict of interest** None.

**Open Access** This article is licensed under a Creative Commons Attribution 4.0 International License, which permits use, sharing, adaptation, distribution and reproduction in any medium or format, as long as you give appropriate credit to the original author(s) and the source, provide a link to the Creative Commons licence, and indicate if changes were made. The images or other third party material in this article are included in the article's Creative Commons licence, unless indicated otherwise in a credit line to the material. If material is not included in the article's Creative Commons licence and your intended use is not permitted by statutory regulation or exceeds the permitted use, you will need to obtain permission directly from the copyright holder. To view a copy of this licence, visit <http://creativecommons.org/licenses/by/4.0/>.

## References

- Adachi M, Hamazawa K, Mimuro Y, Kawamoto H (2017) Vibration transport system for lunar and Martian regolith using dielectric elastomer actuator. *J Electrostat* 89:88–98
- Agui JH, Bucek M, Degennaro A, Wilkinson RA, Zeng X (2013) Lunar excavation experiments in simulant soil test beds: revisiting the surveyor geotechnical data. *J Aerosp Eng* 26(1):117–133
- Agui JH, Wilkinson RA (2010) Granular flow and dynamics of lunar simulants in excavating implements. In: *Earth and space 2010: engineering, science, construction, and operations in challenging environments*: 84–94
- Allton JH (1989) Catalog of Apollo lunar surface geological sampling tools and containers. In: *JSC-23454, LESC-26676*; Lyndon B. Johnson Space Center
- Alshibli KA, Sture S, Costes NC (2001) Constitutive and stability behavior of soils in microgravity environment. In: *AIP conference proceedings* 504(1): 246

6. Anand M, Crawford IA, Balat-Pichelin M, Abanades S, Van Westrenen W, Péraudeau G, Jaumann R, Seboldt W (2012) A brief review of chemical and mineralogical resources on the moon and likely initial in situ resource utilization (ISRU) applications. *Planet Space Sci* 74:42–48
7. Blair BR, Diaz J, Duke MB, Lamassoure E, Easter R, Oderman M, Vaucher M (2002) Space resource economic analysis toolkit: the case for commercial lunar ice mining. In: Final report to the NASA exploration team
8. Briend R, Radziszewski P, Pasini D (2011) Virtual soil calibration for wheel-soil interaction simulations using the discrete-element method. *Can Aeronaut Space Jo* 57(1):59–64
9. Brown JM (1978) Soil excavation improvement from bulldozer blade oscillation. *SAE Trans* 87:2917–2934
10. Burns JO, Duric N, Taylor GJ, Johnson SW (1990) Observatories on the Moon. *Sci Am* 262(3):42–49
11. Carpenter JD, Fisackerly R, Houdou B (2016) Establishing lunar resource viability. *Space Policy* 37:52–57
12. Carrier DW (2003) Particle size distribution of lunar soil. *J Geotech Geoenviron Eng* 129(10):956–959
13. Carrier DW, Olhoeft GR, Mendell W (1991) Physical properties of the lunar surface. In: Heiken GH, Vaniman DT, French BM (eds) *The lunar source book: a user's guide to the moon*. Cambridge University Press, Cambridge, pp 475–595
14. Cockell CS (2010) Astrobiology—what can we do on the moon? *Earth Moon Planet* 107(1):3–10
15. Craft J, Wilson J, Chu P, Zacny K, Davis K (2009) Percussive digging systems for robotic exploration and excavation of planetary and lunar regolith. In: *Proceedings of the 2009 IEEE aerospace conference*. 1152
16. Crawford IA, Elvis M, Carpenter JD (2016) Using extraterrestrial resources for science. *Astron Geophys* 57(4):32–36
17. Crawford IA, Zarnecki J (2008) Astronomy from the moon. *Astron Geophys* 49(2):17–19
18. Ellery A (2016) *Planetary rovers*. Springer, Berlin, Heidelberg. ISBN 9783642032585
19. Ellery A (2018) Lunar in situ resource utilisation—the key to human salvation on earth. *Earth and Space* 2018:380–389
20. Garcet J, Urbina D, Sheridan S, Biswas J, Evagora A, Richter L, Fau G, Kumar H, (2019) Lunar volatiles mobile instrumentation (LUVMI) project results. In: 70th international astronomical congress (IAC). IAC-19-A3.2C.6
21. Goulas A, Friel R (2016) 3D printing with moon dust. *Rapid Prototyp J* 22(6):864–870
22. Green A, Zacny K, Pestana J, Lieu D, Mueller R (2013) Investigating the effects of percussion on excavation forces. *J Aerosp Eng* 26(1):87–96
23. Hadler K, Martin DJP, Carpenter J, Cilliers JJ, Morse A, Starr S, Rasera JN, Seweryn K (2020) A universal framework for space resource utilisation (SRU). In: *Planetary and space science*, Vol. 182, Elsevier Ltd, p 104811. November 2019
24. Hörz F, Grieve R, Heiken G, Spudis P, Binder A (1991) Lunar surface processes. In: Heiken GH, Vaniman D, French BM (eds) *The lunar source book: a user's guide to the moon*. Cambridge University Press, Cambridge, pp 61–1206
25. Iai M, Gertsch L (2013) Excavation of lunar regolith with large grains by rippers for improved excavation efficiency. *J Aerosp Eng* 26(1):97–104
26. Jester S, Falcke H (2009) Science with a lunar low-frequency array: from the dark ages of the universe to nearby exoplanets. *New Astron Rev* 53(1–2):1–26
27. Joy KH, Crawford IA, Curran NM, Zolensky M, Fagan AF, Kring DA (2016) The moon: an archive of small body migration in the solar system. *Earth Moon Planets* 118:133–158
28. Just GH, Joy KH, Roy MJ, Smith KL (2020) Geotechnical characterisation of two new low-fidelity lunar regolith analogues (UoM-B and UoM-W) for use in large-scale engineering experiments. *Acta Astronaut* 173:414–424
29. Just GH, Roy MJ, Joy KH, Hutchings GC, Smith KL (2021) Development and test of a lunar excavation and size separation system (LES3) for the LUVMI-X rover platform. *J Field Robotics* 39(3):263–280
30. Just GH, Smith KL, Joy KH, Roy MJ (2020) Parametric review of existing regolith excavation techniques for lunar in situ resource utilisation (ISRU) and recommendations for future excavation experiments. *Planet Space Sci* 180:104746
31. Kawamoto H (2020) Vibration transport of lunar regolith for in situ resource utilization using piezoelectric actuators with displacement-amplifying mechanism. *J Aerosp Eng* 33(3):04020014
32. Kawamoto H, Shigeta A, Adachi M (2016) Utilizing electrostatic force and mechanical vibration to obtain regolith sample from the moon and mars. *J Aerosp Eng* 29(1):1–6
33. Kawamoto H, Shirai K (2012) Electrostatic transport of lunar soil for in situ resource utilization. *J Aerosp Eng* 25(1):32–138
34. Lavoie AR, Spudis PD (2016) The purpose of human spaceflight and a lunar architecture to explore the potential of resource utilization. In: *SPACE 2016 Conference & Exposition*. 5526
35. Liu Y, Taylor LA (2011) Characterization of lunar dust and a synopsis of available lunar simulants. *Planet Space Sci* 59:1769–1783
36. Lomax BA, Conti M, Khan N, Bennett NS, Ganin AY, Symes MD (2020) Proving the viability of an electrochemical process for the simultaneous extraction of oxygen and production of metal alloys from lunar regolith. *Planet Space Sci* 180:104748
37. Lucey P, Korotev RL, Gillis JJ, Taylor LA, Lawrence D, Campbell BA, Elphic R, Feldman B (2006) Understanding the lunar surface and space-Moon interactions. *Rev Mineral Geochem* 60:83–219
38. McKyes E, Ali OS (1977) The cutting of soil by narrow blades. *J Terramechanics* 14(2):43–58
39. Mueller RP, Smith JD, Lippitt T, Schuler J, Nick A (2013) Reducing extra-terrestrial excavation forces with percussion. In: *Proceedings of the 2013 IEEE aerospace conference*. 1–11
40. Rasera JN, Cilliers JJ, Lamamy J-A, Hadler K (2020) The beneficiation of lunar regolith for space resource utilisation: a review. *Planet Space Sci* 186:104879
41. Sanders GB (2011) Comparison of lunar and Mars in-situ resource utilization for future robotic and human missions. In: 49th AIAA aerospace sciences meeting
42. Sanders GB, Larson WE (2013) Progress made in lunar in situ resource utilization under NASA's exploration technology and development program. *J Aerosp Eng* 26(1):5–17
43. Sargeant HM, Abernethy FAJ, Barber SJ, Wright IP, Anand M, Sheridan S, Morse A (2020) Hydrogen reduction of ilmenite: towards an in situ resource utilization demonstration on the surface of the moon. *Planet Space Sci* 180:104751
44. Seweryn K, Paško P, Visentin Gi (2019) The prototype of regolith sampling tool dedicated to low gravity planetary bodies. *Mech Mach Sci* 73:2711–2720
45. Skonieczny K (2018) Reduced gravity excavation cutting forces considering soil accumulation. *Earth and Space* 2018: 429–439
46. Spudis PD, Lavoie AR (2011) Using the resources of the moon to create a permanent, cislunar space faring system. In: *AIAA SPACE 2011 Conference & Exposition*
47. Sture S, Costes NC, Batiste SN, Lankton MR, AlShibli KA, Jeremias B, Swanson RA, Frank M (1998) Mechanics of granular materials at low effective stresses. *J Aerosp Eng* 11(3):67–72
48. Szabo B, Barnes F, Sture S, Ko H-Y (1998) Effectiveness of vibrating bulldozer and plow blades on draft force reduction. *Trans ASAE* 41(2):283–290

49. Taylor LA, Schmitt HH, Carrier WD, Nakagawa M (January 2005) The lunar dust problem: from liability to asset. In: A collection of technical papers-1st space exploration conference: continuing the voyage of discovery 1: 71–78. ISBN1563477270
50. Vaniman D, Reedy R, Heiken G, Olhoeft G, Mendell W (1991) The lunar environment. In: Lunar sourcebook: a user's guide to the moon. 27–60
51. Wilkinson A, DeGennaro A (2007) Digging and pushing lunar regolith: Classical soil mechanics and the forces needed for excavation and traction. *J Terramechanics* 44(2):133–152
52. Zacny K, Craft J, Hedlund M, Wilson J, Chu P, Funk P, Mueller R, Galloway G (2009) Novel approaches to drilling and excavation on the Moon. In: AIAA SPACE 2009 conference & Exposition, AIAA SPACE Forum
53. Zacny K, Mueller RP, Craft J, Wilson J, Hedlund M, Cohen J (2010) Five-step parametric prediction and optimization tool for lunar surface systems excavation tasks. In: Earth and Space 2010: Engineering, Science, Construction, and Operations in Challenging Environments
54. Zeng X, Burmoski L, Agui JH, Wilkinson (2007) A Calculation of excavation force for ISRU on lunar surface. In: Collection of technical papers-45th AIAA aerospace sciences meeting 24: 17243–17253. ISBN 1563478900
55. Zocca A, Fateri M, Al-Sabbagh D, Günster J (2020) Investigation of the sintering and melting of JSC-2A lunar regolith simulat. *Ceram Int.* <https://doi.org/10.1016/j.ceramint.2020.02.212>
56. Zou M, Fan S, Shi R, Yang Y, Li J (2015) Effect of gravity on the mechanical properties of lunar regolith tested using a low gravity simulation device. *J Terramechanics* 60:11–22

**Publisher's Note** Springer Nature remains neutral with regard to jurisdictional claims in published maps and institutional affiliations.